Structural and physical properties of the new layered transition metal material Na$_4$Cu$_3$TaAs$_4$

Fanbao Meng[1], Mengzhu Shi[1], Shengtao Cui[2], Kunling Peng[1], Naizhou Wang[1], Zhe Sun[2], Jianjun Ying[1] and Xianhui Chen[1,3,4,5*]

ABSTRACT   We report the synthesis, structural and physical properties of a new layered transition metal arsenide Na$_4$Cu$_3$TaAs$_4$. This material adopts the space group $I\bar{4}2m$, with lattice parameters of a=5.9101(3) Å and c=13.8867(12) Å. This structure contains two layers of Na sandwiched by anti-PbO-type (Cu/Ta)As layers, similar to the "111"-type iron-based superconductor NaFeAs. The transition metal sites are occupied by 75% Cu and 25% Ta, with Ta forming a well-defined $\sqrt{2} \times \sqrt{2} \times 2$ superstructure. Cu and Ta were determined to be +1 and +5 oxidation state respectively. The band structure of the Na$_4$Cu$_3$TaAs$_4$ measured by angle resolved photoemission spectroscopy (ARPES) is in good agreement with the density functional theory (DFT) calculation. Both ARPES and resistivity measurement indicate that this material exhibits metallic behavior with p-type carriers. Magnetic susceptibility measurement shows that the material exhibits nearly T-independent diamagnetism. This new material extends the material system with anti-PbO-type layers and offers a good playground to investigate this material system further.

Keywords: layered arsenide, anti-PbO-type layer, superstructure, band structure, physical properties

INTRODUCTION

Layered transition metal materials with anti-PbO-type pnictide or chalcogenide layers have been studied extensively due to their diverse properties. Anti-PbO-type layer can be described as MX (M=transition metal, X=As, P, Se) layer composed of edge-sharing MX$_4$ tetrahedra, which plays a crucial role in physical properties. Among these materials, the most famous one may be the iron-based superconductors with FeAs(Se) layers [1–7], which exhibit unconventional superconductivity with the highest transition temperatures T_c>50 K. Besides high-T_c superconductivity, materials with ani-PbO-type layers also have interesting magnetic [8–11], optical [12] and thermoelectric [13] properties. For example, LaOMnAs with MnAs layers exhibits large negative magnetoresistance [10].

In addition, materials with variants of the anti-PbO-type MX layer also have been studied extensively. One of the variants is [MSe$_2$]$^{2-}$-type layer in Ln$_2$O$_2$MSe$_2$ (Ln=La, Ce), which is induced by half-occupancy of the transition-metal and exhibits diverse cation-ordered structures. For example, in La$_2$O$_2$CdSe$_2$ with [CdSe$_2$]$^{2-}$, Cd^{2+} cations occupy alternate tetrahedral sites, forming a $\sqrt{2} \times \sqrt{2}$ superstructure in the ab plane relative to perfect anti-PbO-type MX layer [14]. Whereas in La$_2$O$_2$FeSe$_2$, [FeSe$_2$]$^{2-}$ layers contain 1D chains of edge-sharing (stripe-like) FeSe$_4$ tetrahedra [15]. This kind of variant can be considered as anti-PbO-type MX layers composed by ordered transition metal elements and vacancies. Another variant is MX layer composed by two kinds of transition metal elements, which also exhibits cation-ordered structure. Materials containing this kind of variant are rare. Only one compound, NaFe$_{0.5}$Cu$_{0.5}$As, has been reported, in which Fe^{3+} and Cu^{1+} arrange orderly, forming 2×2 superstructure [16]. Except for Fe and Cu ordering, NaFe$_{0.5}$Cu$_{0.5}$As also exhibits antiferromagnetic Mott-insulating state which connects with high-T_c superconductivity. Considering the interesting structural fea-

[1] Key Laboratory of Strongly Coupled Quantum Matter Physics, Chinese Academy of Sciences, Hefei National Laboratory for Physical Sciences at Microscale, Department of Physics, University of Science and Technology of China, Hefei 230026, China
[2] National Synchrotron Radiation Laboratory, University of Science and Technology of China, Hefei 230026, China
[3] Collaborative Innovation Center of Advanced Microstructures, Nanjing University, Nanjing 210093, China
[4] CAS Center for Excellence in Superconducting Electronics (CENSE), Shanghai 200050, China
[5] CAS Center for Excellence in Quantum Information and Quantum Physics, Hefei 230026, China
* Corresponding author (email: chenxh@ustc.edu.cn)

tures and physical properties of this kind of material, more work is needed to explore this material system.

In our current research, we synthesized a new layered $Na_4Cu_3TaAs_4$ single crystal with anti-PbO-type (Cu/Ta)As layers composed by ordered Cu and Ta. The crystal structure of the new material was determined by single crystal X-ray diffraction (XRD) technique. Ta forms $\sqrt{2} \times \sqrt{2} \times 2$ superstructure. Cu and Ta were determined to be +1 and +5 oxidation state by X-ray photoelectron spectroscopy (XPS) respectively. The dispersion relations measured by angle resolved photoemission spectroscopy (ARPES) are in good agreement with theoretical calculation. ARPES and resistivity measurement both show that the new material exhibits metallic behavior. And magnetic susceptibility measurement indicates that the new material exhibits diamagnetism.

EXPERIMENTAL SECTION

Synthesis and analysis

High-quality $Na_4Cu_3TaAs_4$ single crystal was grown by a self-flux technique which was similar to the synthesis method of $NaFe_{1-x}Co_xAs$ [17]. The single crystal was commenced from the elements, handled in an argon-filled glovebox. The NaAs was used as flux to synthesize the sample. Firstly, NaAs precursor was prepared. Na pieces and As powder ground from As lumps were weighted at the molar ratio of 1:1 and sealed in quartz ampoule, then reacted at 200°C for 10 h. Secondly, the NaAs precursor was mixed with the Cu powder (Alfa Aesar, ~600 mesh, 99.5%) and Ta powder (Alfa Aesar, ~100 mesh, 99.5%) at the molar ratio of Na:As:Cu: Ta=4:4:0.75:0.25. The mixture was thoroughly ground and sealed in tantalum crucibles. Then the crucibles were sealed in a quartz tube under a vacuum of approximately 1×10^{-3} mbar. Thirdly, the reaction was conducted in a pit furnace to get high quality single crystals. The quartz tubes were heated to 950°C at the rate of 100°C/h and kept at this temperature for 10 h and then cooled to 650°C at the rate of 3°C/h. Finally, high-quality single crystals could be picked from NaAs flux easily. The single crystals can be cleaved and the sizes of the single crystals were typically 3 mm×2 mm×0.3 mm. We could cleave the single crystals by using a blade to obtain fresh and clean surface for measurements. Both single-crystal and polycrystalline samples were used in this study. The polycrystalline samples were prepared by crushing the single crystal into fragments thoroughly in the glove box. It is worthy to note that the $Na_4Cu_3TaAs_4$ single crystals are

sensitive to air and moisture. In order to obtain intrinsic physical properties, the samples must be stored and transported in sealed containers filled with an insert gas.

The single-crystal and polycrystalline samples were characterized by X-ray diffractometer (Smartlab-9, Rigaku Corp) with Cu Kα radiation and a fixed graphite monochromator in the range of 10°–70° at room temperature.

To determine the actual chemical composition of the single crystal, energy-dispersive X-ray analysis (EDX) was performed on the single crystal by using the field emission scanning electron microscope (FE-SEM SIRION 200) with an additional EDX device. The ratio of Na, Cu, Ta and As was determined to be 32.943:25.590:8.771: 32.697 (in atom%). And the chemical formula could be identified as $Na_4Cu_3TaAs_4$ (i.e., $NaCu_{0.75}Ta_{0.25}As$). Any additional elements were not found. The EDX spectra and chemical compositions at different areas of the $Na_4Cu_3TaAs_4$ single crystals are shown in Fig. S1 and Table S1 (see Supplementary information (SI)).

The valences of Cu, Ta, As and Na in the single crystal were determined with XPS by using an ESCAlab250 XPS with monochromatized Al Kα X-ray source.

Crystal structure determinations

A single crystal XRD technique was also performed to give insight into atomic crystal structures. A shinny single crystal with the size of 0.2 mm×0.1 mm×0.03 mm was selected using the microscope and then mounted on a glass fiber. Single crystal XRD data were collected by using an Oxford Diffraction Gemini S Ultra CCD diffractometer equipped with graphite-monochromatized Mo Kα (λ=0.7107 Å) radiation at 293 K. Then the crystal structures were resolved by direct methods and the data refinement was done by using the full-matrix least-squares methods with SHELXL-2018 programs [18].

Calculation of the band structure

The projector augmented plane wave (PAW) [19,20] method as implemented in the Vienna ab initio simulation package (VASP) [21] code was used for structure relaxation. The exchange-correlation function was defined by using a generalized gradient approximation (GGA) of Perdew-Burke-Ernzerhof (PBE) [22]. The total energies were numerically converged to 1×10^{-6} eV by using a kinetic energy cutoff of 500 eV. The atomic positions were relaxed until the forces on the atoms were smaller than 0.01 eV Å^{-1}. For the Brillouin zone integrations, we used the Monkhorst-Park k-mesh scheme with 9×9×9 for the primitive cell ($I\bar{4}2m$, 12 atoms).

Physical property measurements

ARPES experiments were performed with 90 eV photos at the beamline 13U of the National Synchrotron Radiation Laboratory (NSRL) at Hefei, China, by using a Scienta R4000 electron spectrometer. All samples were cleaved *in situ* and measured at 300 K under a vacuum less than 5 $\times 10^{-11}$ mbar. The temperature dependence of resistivity was measured by a standard four-probe method. Because the single crystal was sensitive to the air, the electrodes were made in the glove box with high pure Argon gas and the electrical transport measurement was conducted on PPMS-9 T (Quantum Design). The magnetic suscept-ibility was measured by a SQUID magnetometer (MPMS-5 T, Quantum Design).

RESULTS

The single crystal and polycrystalline XRD patterns of $Na_4Cu_3TaAs_4$ collected at room temperature are shown in Fig. 1. As shown in Fig. 1a, the XRD pattern of $Na_4Cu_3TaAs_4$ single crystal sample exhibits a highly (001)

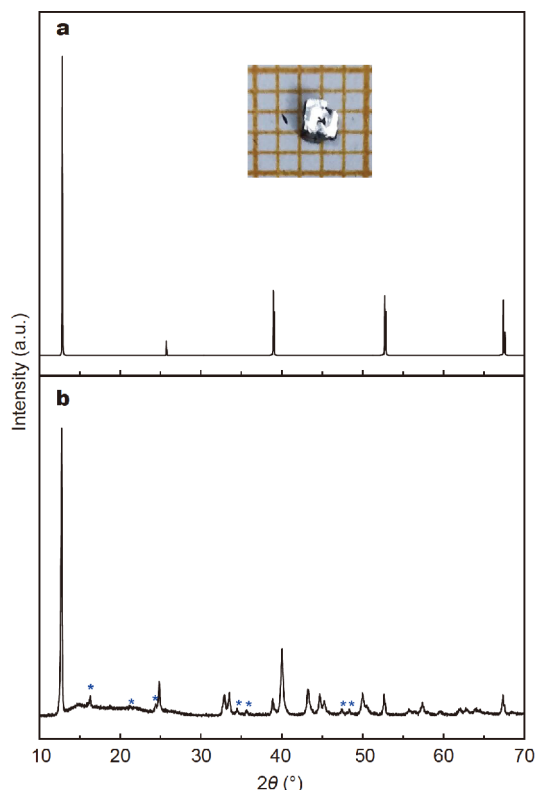orientation, indicating that the single crystal is of high quality. The polycrystalline XRD pattern shown in Fig. 1b is similar to that of known "111"-type Fe-based super-conductor [23]. And the main diffraction peaks in the XRD pattern can be well indexed by the structure of NaFeAs except for some peaks with relatively weak in-tensity (blue stars), demonstrating that the new material has the same basic structure as NaFeAs. Therefore, the chemical formula of the new material can be written as $NaCu_{0.75}Ta_{0.25}As$, in which equivalently 25% Cu is re-placed by Ta in the parent compound "NaCuAs", al-though the parent cannot be synthesized yet. And these excrescent weak peaks may stem from orderly arrange-ment of Ta, which is similar to superstructure peaks in $NaFe_{1-x}Cu_xAs$ originating from Cu cations doping [16] and $K_2Fe_4Se_5$ originating from the ordered vacancies of the Fe [24,25].

In order to determine the accurate crystal structure of $Na_4Cu_3TaAs_4$, we performed further structural in-vestigation by means of single crystal XRD technique. The resulting structure is shown in Fig. 2. The crystal structure of $Na_4Cu_3TaAs_4$ has five independent crystal-lographic positions: two positions are occupied by Cu, one position occupied by Na, one position occupied by Ta and the remaining one occupied by As. The crystal-lographic data of $Na_4Cu_3TaAs_4$ is shown in Table 1. The atomic positions and displacement parameters are sum-marized in Table 2. And the interatomic distances are
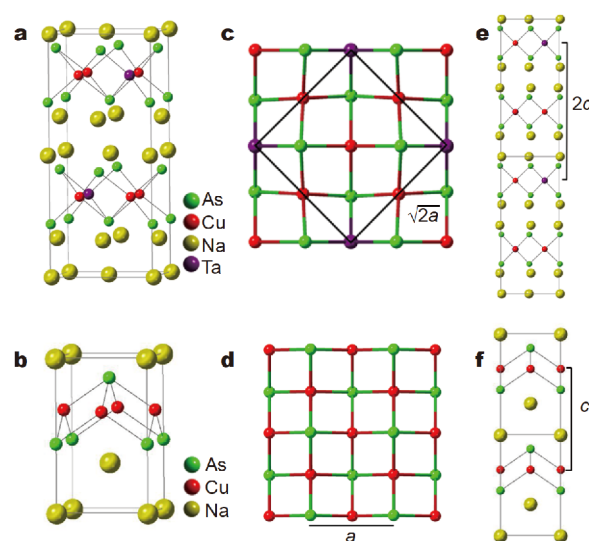

Figure 1 The XRD patterns taken from $Na_4Cu_3TaAs_4$ single crystal and polycrystalline samples. (a) The single crystal XRD pattern shows a series of (001) diffractions. The inset shows the photograph of the single crystal. (b) The powder XRD pattern. Excrescent peaks compared to NaFeAs are marked with blue asterisks.

Figure 2 The structure of $Na_4Cu_3TaAs_4$ and "parent" NaCuAs. (a, b) Schematic illustration of the crystal structure of the $Na_4Cu_3TaAs_4$ and "NaCuAs". (c, d) (Cu/Ta)As nets of the $Na_4Cu_3TaAs_4$ and CuAs nets of the "NaCuAs" in the *ab* plane. (e, f) Structures of the $Na_4Cu_3TaAs_4$ and the "NaCuAs" along the *c* direction.

Parameters	Values
Chemical formula	Na$_4$Cu$_3$TaAs$_4$
Formula weight (g mol^{-1})	763.21
Temperature (K)	293(2) K
Wavelength (Å)	0.71073
Crystal system	Tetragonal
Space group	$I\bar{4}2m$(121)
a (Å)	5.9101(3)
b (Å)	5.9101(3)
c (Å)	13.8867(12)
α (°)	90
β (°)	90
γ (°)	90
V (Å^3)	485.05(6)
Z	2
Density (g cm^{-3})	5.226
Abs coeff (mm^{-1})	31.371
F(000)	672
GOF on F^2	1.114
R_1 and wR_2 (all data)^a	0.0587, 0.1396
R_1 and wR_2 ($I>2\sigma(I)$)^a	0.0571, 0.1384

a) $R_1(F) = \sum \left| |F_o| - |F_c| \right| / \sum |F_o|$,

$wR_2\left(F_o^2\right) = \left[\sum w \left(F_o^2 - F_c^2 \right)^2 / \sum w \left(F_o^2 \right)^2 \right]^{1/2}$.

summarized in Table S2.

As shown in Fig. 2a and b, Na$_4$Cu$_3$TaAs$_4$ can be regarded to share similar structure with NaFeAs ("NaCuAs"). The crystal structure of Na$_4$Cu$_3$TaAs$_4$ is constituted by double layers of Na cations sandwiched by anti-PbO-type (Cu/Ta)As layer which is the same as FeAs layer in NaFeAs. The stacking sequence along the c axis is As-(Cu/Ta)-As-Na-Na-As.

Further analyzing the crystal structure, we find Ta arranges orderly. As shown in Fig. 2c–f, compared with the possible parent compound "NaCuAs", Ta in the (Cu/Ta)As layer forms a $\sqrt{2} \times \sqrt{2} \times 2$ superstructure re-

lative to perfect CuAs layer in "NaCuAs". In the ab plane, the distance of adjacent Ta is $\sqrt{2}$ times that of adjacent Cu. Along the c axis, the distance of adjacent Ta is twice that of adjacent Cu. In fact, compounds with perfect anti-PbO-type CuAs layer have been already synthesized, such as SrCu$_2$As$_2$ [26]. While SrCu$_2$As$_2$ is a typical 122-type compound. Compared with SrCu$_2$As$_2$, 25% Cu is replaced by ordered Ta, and single layer of Sr sandwiched by CuAs layers in SrCu$_2$As$_2$ is replaced by double layers of Na. Due to orderly arrangement of Ta, the crystal structure reduces symmetry and adopts the $I\bar{4}2m$ (121) space group. And the lattice constants of Na$_4$Cu$_3$TaAs$_4$ are $a=$ 5.9101(3) Å and $c=$13.8867(12) Å. Thus, all peaks in the polycrystalline XRD pattern can be indexed with the new structure (see Fig. S2 in SI). And the polycrystalline XRD Rietveld refinement result is summarized in Table S3.

In order to investigate the electronic structure of the Na$_4$Cu$_3$TaAs$_4$, we carried out XPS measurement on the single crystal samples. Fig. 3 shows the Cu 2p, Ta 4f, As 3d regions in the spectrum of Na$_4$Cu$_3$TaAs$_4$. As shown in Fig. 3a, we compare the Cu valance of Na$_4$Cu$_3$TaAs$_4$ with those of CuO and SrCu$_2$As$_2$ samples. The peak positions of Cu 2p$_{1/2}$ and Cu 2p$_{3/2}$ are at about 952.0 and 932.0 eV respectively. The peak positions of Cu for the Na$_4$Cu$_3$TaAs$_4$ single crystal are nearly the same as SrCu$_2$As$_2$ [27]. While the peak positions for divalent copper in CuO sample shift to higher binding energy, which are distinctly different from those of Cu^{1+}. In addition, the XPS pattern of divalent copper has very intense satellite peak. Based on these, we determine that the valance state of Cu in the Na$_4$Cu$_3$TaAs$_4$ is +1 oxidation state with fully occupied 3d^{10} configuration. For the Ta 4f region, after the background was deduced with the Shirley function, two peaks could be observed. As shown in Fig. 3b, the low binding energy of Ta 4f$_{7/2}$ peak at 25.5 eV is slightly lower than that of Ta$_2$O$_5$ (26.5 eV), but much higher than that of TaS$_2$ (23.60 eV). Therefore, the valence of Ta is extremely close to +5. For the As 3d region, only one peak could be observed at 40.29 eV. The binding energy of As 3d is in accordance with the binding energy of GaAs and the valance is −3. And the valance of

Table 2   Atomic coordinates and equivalent displacement parameters for Na$_4$Cu$_3$TaAs$_4$

Atom	Wyckoff	x	y	z	Occup	U_{eq} (Å^2)
Na1	8i	0.7329(16)	0.7329(16)	0.8259(9)	1	0.023(3)
Cu1	4c	0.5	1	0.5	1	0.017(2)
Cu2	2b	1	1	0.5	1	0.045(2)
Ta1	2a	0.5	0.5	0.5	1	0.01(1)
As1	8i	0.7381(4)	0.7381(4)	0.6069(2)	1	0.014(1)
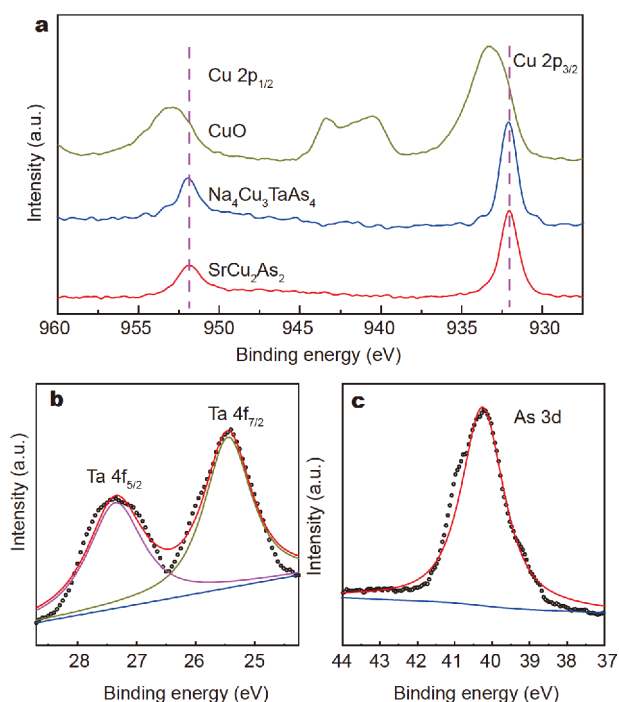
Figure 3 The XPS spectrum for $Na_4Cu_3TaAs_4$. (a) The region of Cu $2p_{1/2}$ and Cu $2p_{3/2}$, compared with CuO and $SrCu_2As_2$ single crystals. (b) The region of Ta $4f_{5/2}$ and Ta $4f_{7/2}$. (c) The region of As $3d$.

Na is +1 (see Fig. S3 in SI).

Then we determined the band structure of $Na_4Cu_3TaAs_4$ by ARPES. The ARPES-intensity plot along the Γ-M-A cut in the Brillouin-zone for $Na_4Cu_3TaAs_4$ single crystal at room temperature is shown in Fig. 4a. The calculated band structure for $Na_4Cu_3TaAs_4$ is shown in Fig. 4b. As seen in Fig. 4a and b, the experimental dispersion relations are in good agreement with theoretical calculation. ARPES along the Γ-M direction in Fig. 4a shows the hole-like bands centered at the M point.
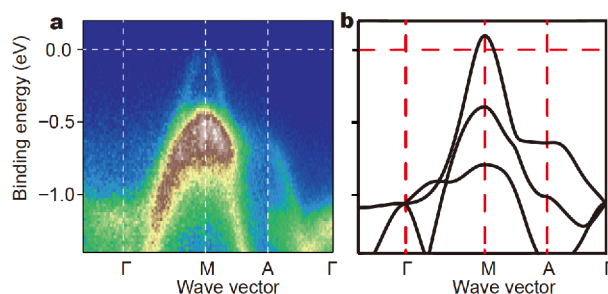
Figure 4 The electronic structure of $Na_4Cu_3TaAs_4$. (a) Valence-band ARPES intensity of $Na_4Cu_3TaAs_4$ measured along the Γ-M-A cut at room temperature. (b) Calculated band structure obtained from the first-principles band-structure calculations for $Na_4Cu_3TaAs_4$.

Fermi surface crosses the energy band, indicating that $Na_4Cu_3TaAs_4$ is metallic with hole carriers. And the hole carrier concentration is estimated to be of the order of 10^{19} cm^{-3} according to the band structure.

The transport property and magnetic susceptibility of $Na_4Cu_3TaAs_4$ single crystal are shown in Fig. 5. Fig. 5a shows the in-plane resistivity ρ as a function of temperature over the range from 300 to 2 K. According to the results, the temperature dependence of the resistivity indicates that the single crystal is metallic. And there is no superconductivity or other apparent phase transition down to 2 K. At room temperature, the resistivity is about 10.78 mΩ cm. We fit the resistivity data to the equation $\rho=a+bT^2$ in the temperature range 5–100 K and obtain value of n=1.934 which is close to 2, suggesting Fermi liquid behavior. The temperature dependence of the Hall coefficient (R_H) and carrier concentration (n) are shown in the inset of Fig. 5a. The value of R_H is positive in the whole temperature range, which implies that hole-type charge carriers dominate the conduction in the $Na_4Cu_3TaAs_4$. The carrier concentration is estimated to
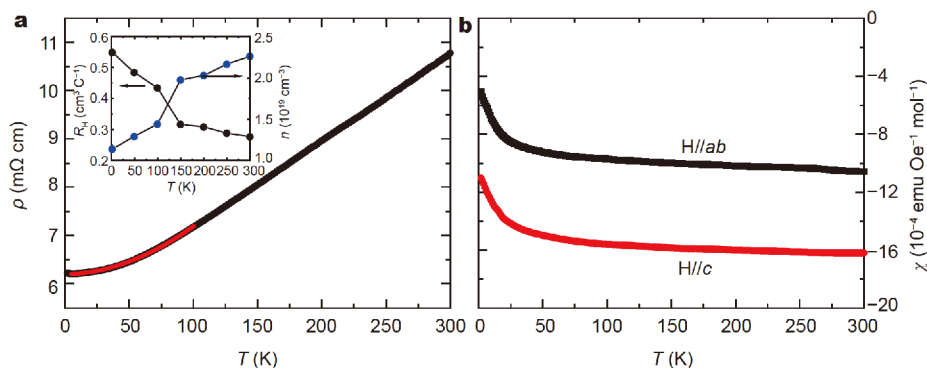

Figure 5 Resistivity and magnetic susceptibility of single crystal $Na_4Cu_3TaAs_4$. (a) The temperature dependence of in-plane resistivity for the single crystal. The solid red curve is a fit of the resistivity in the temperature range 5–100 K. Inset: the temperature dependence of Hall coefficient (R_H) and carriers concentration (n) at 2–300 K. (b) The temperature dependence of ZFC magnetic susceptibility for the single crystal at a magnetic field of 5 T applied along the c axis (χ_c, H//c) and in the ab plane (χ_{ab}, H//ab).

be of the order of 10^{19} cm^{-3} by $n=1/R_{H}e$ using the single carrier model. The metallic feature and carrier concentration are consistent with the results estimated from ARPES. The lower carrier concentration is responsible for the larger resistivity.

The temperature dependence of zero-field-cooled (ZFC) magnetic susceptibility $\chi=M/H$ of the Na$_4$Cu$_3$TaAs$_4$ single crystal from 2 to 300 K under an external field is presented in Fig. 5b, where M is the measured magnetization of the Na$_4$Cu$_3$TaAs$_4$ single crystal. The applied field H of 5 T was aligned along the c axis (χ_c, H//c) and in the ab plane (χ_{ab}, H//ab). The $\chi(T)$ of the single crystal for both χ_{ab} and χ_c are negative and an obvious anisotropy with $\chi_{ab} > \chi_c$ is observed over the whole measured temperature range. The negative susceptibility and anisotropy are similar to that of copper arsenide SrCu$_2$As$_2$ [26]. The $\chi(T)$ of the single crystal in Fig. 5b shows weak temperature dependence without apparent magnetic transition down to 2 K, which means there is no long range magnetic order in this material. Small Curie-Weiss tails are observed at low temperature for both χ_{ab} and χ_c, probably due to the contribution of a small quantity of paramagnetic impurities in the sample. Absence of long range magnetic order is consistent with nonmagnetic +1 oxidation state of Cu and +5 oxidation state of Ta.

DISCUSSION

The Cu^{1+} oxidation state and 3d^{10} electronic configuration are relatively stable, and the oxidability of arsenic is not strong enough to oxidize Cu to +2 oxidation state, so it is not strange that Cu in Na$_4$Cu$_3$TaAs$_4$ has +1 oxidation state. In addition, according to the survey of the radii of the elements by Cordero *et al.* [28], As–As covalent bond distance is 2.38(8) Å. In SrCu$_2$As$_2$ with anti-PbO type CuAs layer, the value d_{As-As}=2.470 Å is close to the As–As covalent bond distance, yielding As^{2-} oxidation state (As^{-2}=[As–As]$^{-4}$/2). However, for Na$_4$Cu$_3$TaAs$_4$, the distance of As–As is 4.961 Å. The value is too large to prevent the formation of As–As covalent bond, which confirms that the oxidation state of As in this material is As^{3-} as discussed above. Therefore the crystal "NaCuAs" cannot be stabilized. But when 25% Cu^{1+} are replaced by Ta^{5+}, the structure can be stabilized because of realizing balance of valence state. In addition, according to the Shannon's tables [29], the ionic radii values of Cu^{1+} and Ta^{5+} are 0.60 and 0.64 Å respectively. Their ionic radii values are very close, contributing to stabilizing the structure. In the materials with variants of anti-PbO-type layers, including Ln$_2$O$_2$MSe$_2$ [30], NaFe$_{0.5}$Cu$_{0.5}$As and

K$_2$Fe$_4$Se$_5$, transition metal ions or vacancies usually arrange orderly. This phenomenon makes us speculate that the superstructure induced by transition metal ordered arrangement in anti-PbO-type layer may be a kind of advantageous mode contributing to stabilizing the structure [30].

CONCLUSIONS

In summary, a new transition metal layered material, Na$_4$Cu$_3$TaAs$_4$ single crystal, has been synthesized by a self-flux technique. This new material has layered structure, containing two layers of Na sandwiched by anti-PbO-type (Cu/Ta)As layers. And in (Cu/Ta)As layers, Ta forms $\sqrt{2} \times \sqrt{2} \times 2$ superstructure compared with the related 111 type iron-based superconductor. Cu in the Na$_4$Cu$_3$TaAs$_4$ is +1 oxidation state with a fully occupied 3d^{10} configuration and Ta is +5 oxidation state with 4f^{14} electronic configuration. The valence and electronic configuration of Cu and Ta is the key to the structure stabilization. The band structure measured by ARPES is in good agreement with DFT calculation. And this material exhibits metallic behavior with p-type carriers and T-independent diamagnetic behavior.

1. Kamihara Y, Watanabe T, Hirano M, *et al.* Iron-based layered superconductor La[O$_{1-x}$F$_x$]FeAs (x=0.05–0.12) with T_c=26 K. J Am Chem Soc, 2008, 130: 3296–3297

2. Chen XH, Wu T, Wu G, *et al.* Superconductivity at 43 K in SmFeAsO$_{1-x}$F$_x$. Nature, 2008, 453: 761–762

3. Ren ZA, Lu W, Yang J, *et al.* Superconductivity at 55 K in iron-based F-doped layered quaternary compound Sm[O$_{1-x}$F$_x$]FeAs. Chin Phys Lett, 2008, 25: 2215–2216

4. Rotter M, Tegel M, Johrendt D. Superconductivity at 38 K in the iron arsenide Ba$_{1-x}$K$_x$Fe$_2$As$_2$. Phys Rev Lett, 2008, 101: 107006

5. Parker DR, Pitcher MJ, Baker PJ, *et al.* Structure, anti-ferromagnetism and superconductivity of the layered iron arsenide NaFeAs. Chem Commun, 2009, 16: 2189–2191

6. Hsu FC, Luo JY, Yeh KW, *et al.* Superconductivity in the PbO-type structure α-FeSe. Proc Natl Acad Sci USA, 2008, 105: 14262–14264

7. Guo J, Jin S, Wang G, *et al.* Superconductivity in the iron selenide K$_x$Fe$_2$Se$_2$ (0<x<1.0). Phys Rev B, 2010, 82: 180520

8. Yanagi H, Kawamura R, Kamiya T, *et al.* Itinerant ferromagnetism in the layered crystals LaCoOX (X=P, As). Phys Rev B, 2008, 77: 224431

9. Sefat AS, Singh DJ, Jin R, *et al.* Renormalized behavior and proximity of BaCo$_2$As$_2$ to a magnetic quantum critical point. Phys Rev B, 2009, 79: 024512

10. Emery N, Wildman EJ, Skakle JMS, *et al.* Giant magnetoresistance in oxypnictides (La,Nd)OMnAs. Chem Commun, 2010, 46: 6777–6779

11. Singh Y, Ellern A, Johnston DC. Magnetic, transport, and thermal properties of single crystals of the layered arsenide BaMn$_2$As$_2$. Phys

Rev B, 2009, 79: 094519

12　Ueda K, Inoue S, Hirose S, et al. Transparent p-type semiconductor: LaCuOS layered oxysulfide. Appl Phys Lett, 2000, 77: 2701–2703

13　Barreteau C, Pan L, Amzallag E, et al. Layered oxychalcogenide in the Bi-Cu-O-Se system as good thermoelectric materials. Semicond Sci Technol, 2014, 29: 064001

14　Hiramatsu H, Ueda K, Kamiya T, et al. Synthesis of single-phase layered oxychalcogenide $La_2CdO_2Se_2$: Crystal structure, optical and electrical properties. J Mater Chem, 2004, 14: 2946–2950

15　McCabe EE, Free DG, Evans JSO. A new iron oxyselenide $Ce_2O_2FeSe_2$: Synthesis and characterisation. Chem Commun, 2011, 47: 1261–1263

16　Song Y, Yamani Z, Cao C, et al. A Mott insulator continuously connected to iron pnictide superconductors. Nat Commun, 2016, 7: 13879

17　Wang AF, Luo XG, Yan YJ, et al. Phase diagram and calorimetric properties of $NaFe_{1-x}Co_xAs$. Phys Rev B, 2012, 85: 224521

18　Sheldrick GM. SHELXS-2018, Programs for X-ray Crystal Structure Solution. Göttingen: University of Göttingen, 2018

19　Blöchl PE. Projector augmented-wave method. Phys Rev B, 1994, 50: 17953–17979

20　Kresse G, Joubert D. From ultrasoft pseudopotentials to the projector augmented-wave method. Phys Rev B, 1999, 59: 1758–1775

21　Kresse G, Furthmüller J. Efficient iterative schemes for ab initio total-energy calculations using a plane-wave basis set. Phys Rev B, 1996, 54: 11169–11186

22　Perdew JP, Burke K, Ernzerhof M. Generalized gradient approximation made simple. Phys Rev Lett, 1996, 77: 3865–3868

23　Chu CW, Chen F, Gooch M, et al. The synthesis and characterization of LiFeAs and NaFeAs. Phys C-Supercond, 2009, 469: 326–331

24　Zavalij P, Bao W, Wang XF, et al. Structure of vacancy-ordered single-crystalline superconducting potassium iron selenide. Phys Rev B, 2011, 83: 132509

25　Song YJ, Wang Z, Wang ZW, et al. Phase transition, superstructure and physical properties of $K_2Fe_4Se_5$. EPL, 2011, 95: 37007

26　Anand VK, Perera PK, Pandey A, et al. Crystal growth and physical properties of $SrCu_2As_2$, $SrCu_2Sb_2$, and $BaCu_2Sb_2$. Phys Rev B, 2012, 85: 214523

27　Yan YJ, Cheng P, Ying JJ, et al. Structural, magnetic, and electronic transport properties of hole-doped $SrFe_{2-x}Cu_xAs_2$ single crystals. Phys Rev B, 2013, 87: 075105

28　Cordero B, Gómez V, Platero-Prats AE, et al. Covalent radii revisited. Dalton Trans, 2008, 21: 2832–2838

29　Shannon RD. Revised effective ionic radii and systematic studies of interatomic distances in halides and chalcogenides. Acta Cryst A, 1976, 32: 751–767

30　Ainsworth CM, Wang CH, Johnston HE, et al. Infinitely adaptive transition-metal ordering in $Ln_2O_2MSe_2$-type oxychalcogenides. Inorg Chem, 2015, 54: 7230–7238

Fanbao Meng obtained his Bachelor degree in physics from Zhengzhou Universtiy. He is currently a PhD candidate in the University of Science and Technology of China (USTC) under the supervision of Prof. Xianhui Chen. His current research interest focuses on the exploration and characterization of layered functional material.

Xianhui Chen obtained his PhD degree in physics from USTC in 1992. In the same year, he began his research career in USTC and now holds the position of Professor in physics. His research focuses on the exploration and study of the physics of novel functional materials exhibiting superconductivity, novel magnetism, novel quantum properties, thermoelectricity, etc.

一种新的过渡金属层状材料$Na_4Cu_3TaAs_4$的结构和物理性质

孟凡保[1]，石梦竹[1]，崔胜涛[2]，彭坤岭[1]，王乃舟[1]，孙喆[2]，应剑俊[1]，陈仙辉[1,3,4,5*]

摘要　我们报道了一种新的过渡金属层状砷化物$Na_4Cu_3TaAs_4$的合成、结构和物理性质。这种材料采用$I\bar{4}2m$空间群，晶胞参数为a=5.9101(3) Å，c=13.8867(12) Å。这个材料的结构中包含两层Na，而Na夹在反氧化铅型(Cu/Ta)As层之间，类似于"111"型铁基超导体NaFeAs。过渡金属位由75%的Cu和25%的Ta占据，Ta形成了明确的$\sqrt{2} \times \sqrt{2} \times 2$超结构。Cu和Ta分别为+1和+5价。角分辨光电子能谱测得的$Na_4Cu_3TaAs_4$能带结构能够和DFT计算结果良好地吻合。角分辨光电子能谱和输运测量均表明该材料表现为金属行为，具有p型载流子。磁化率测量表明该材料表现为几乎不依赖温度的抗磁性。这种新材料扩展了含有反氧化铅型层的材料系统，并为进一步研究该材料系统提供了一个很好的平台。